

Human Body as Antenna and Its Effect on Human Body Communications

Behailu Kibret*, Assefa K. Teshome, and Daniel T. H. Lai

Abstract—Human body communication (HBC) is a promising wireless technology that uses the human body as part of the communication channel. HBC operates in the near-field of the high frequency (HF) band and in the lower frequencies of the very high frequency (VHF) band, where the electromagnetic field has the tendency to be confined inside the human body. Electromagnetic interference poses a serious reliability issue in HBC; consequently, it has been given increasing attention in regard to adapting techniques to curtail its degrading effect. Nevertheless, there is a gap in knowledge on the mechanism of HBC interference that is prompted when the human body is exposed to electromagnetic fields as well as the effect of the human body as an antenna on HBC. This paper narrows the gap by introducing the mechanisms of HBC interference caused by electromagnetic field exposure of human body. We derived analytic expressions for induced total axial current in the body and associated fields in the vicinity of the body when an imperfectly conducting cylindrical antenna model of the human body is illuminated by a vertically polarized plane wave within the 1–200 MHz frequency range. Also, fields in the vicinity of the human body model from an on-body HBC transmitter are calculated. Furthermore, conducted electromagnetic interference on externally embedded HBC receivers is also addressed. The results show that the maximum HBC gain near 50 MHz is due to whole-body resonance, and the maximum at 80 MHz is due to the resonance of the arm. Similarly, the results also suggest that the magnitude of induced axial current in the body due to electromagnetic field exposure of human body is higher near 50 MHz.

1. INTRODUCTION

Human body communication (HBC)/Intrabody communication (IBC)/Body channel communication (BCC) is an emerging wireless communication technique that uses the human body as a transmission medium to connect wearable biomedical sensor nodes and electronic devices in a wireless body area network (WBAN). The human body acts as a waveguide in the frequency range of hundreds of kHz to dozens of MHz, which is considered suitable for HBC operation. More specifically, IEEE 802.15.6 defines 21 MHz as center frequency for HBC. HBC uses near-field coupling that leads to low radiation to free space; as a result, it promises a secured low data rate communication. Due to the low propagation loss, it also promises higher communication performance compared to other body area communication techniques, such as ultra wideband (UWB) [1].

In the literature, two approaches of HBC are widely discussed [2]. In the first approach, the transmitter uses two electrodes, which are attached to the body, to differentially couple modulated current into the body, resulting in a gradient of electric potential around it. The receiver detects the signal from the potential difference between another pair of electrodes attached to the body. This type of approach is commonly called galvanic coupling HBC. In the second approach, the transmitter couples electric current into the body using a single on-body electrode and the receiver also detects the signal using a single on-body electrode. A return path is established through the vicinity of the human body

Received 12 June 2014, Accepted 2 August 2014, Scheduled 19 August 2014

* Corresponding author: Behailu Kibret (behailu.kibret@live.vu.edu.au).

The authors are with the College of Engineering and Science, Victoria University, Melbourne, Australia.

with near-field coupling of the transmitter and receiver circuit ground planes. This type of approach is usually referred to as capacitive or near-field coupling HBC.

There is a prevalent claim that HBC provides a secure and interference immune channel, which is hypothesised, based on the assumption that the signal is physically guarded by the human body and electromagnetic radiation is low [1, 3, 4]. This view is not always valid. For efficient low power and high frequency operation, one of the constraints in HBC transceiver design is ensuring most of the signal is coupled to the body as electric current or confined to the vicinity of human body as reactive near-field. This leads to a reduction of power lost due to radiation into free space and due to mutual coupling with nearby objects. The natural approach to achieve this is through the use of coupling electrodes that are in direct contact with the body instead of using a traditional RF antenna. It can also be further improved by scaling the HBC circuit to a dimension that is very small compared to wavelength of the signal coupled to the body, and at the same time optimizing the size of circuit ground planes for good near-field coupling. This implies that properly designed HBC devices might not be good RF radiation sources, which in turn means that they might not also be good receiving antennas for external electromagnetic disturbances within the HBC operation frequency. Such notions of HBC seemingly classify it as a wireless technique that is less sensitive to RF interference. Even though HBC devices are poor RF antennas, there is another mechanism of electromagnetic interference (EMI) that threatens the operation of HBC. Since HBC operates on the surface of the human body, the current induced in the body due to RF exposure may interfere with body-worn devices. In other words, the human body can act like a receiving antenna, which indirectly affects the HBC channel. From reciprocity, the reverse is also true — the human body can also act as transmitting antenna due to the HBC induced current inside the body - this could impact security.

In the literature, there are only a few studies that addressed interference problems posed by the human body acting as an antenna. The seriousness of reliability issue in HBC arising from interference caused by human body as a receiving antenna is discussed in [5]. From measured RF interference power, a specific case was reported that showed the signal-to-interference ratio (SIR) of HBC degrades to -22 dB. Based on this, the paper proposed an adaptive frequency hopping technique to improve the SIR. In a similar work [4], the electric field strength around the human subject wearing HBC transceivers was measured with an antenna located 3m away to determine the effects of nearby RF devices. The study reported irregular radiation patterns and unpredictable directivity at different frequencies, which are typical near-field phenomena possibly affected by mutual coupling of the subject, the measuring antenna and nearby objects. Another study [6] investigated the effect of EMI on implanted medical devices, specifically cardiac pacemakers, due to the electromagnetic field from on-body HBC transmitter. Park et al. [7] proposed the digital communication technique of frequency selective baseband transmission (FSBT) for HBC in order to cope with the reliability issue posed by interference. Anguera et al. showed that the human body can act as an efficient FM (100 MHz) antenna demonstrating that the efficiency of an electrically small antenna in some cases can be improved up to 10 dB, approximately [8–11]. Overall, little has been reported in the literature on the mechanism of human body antenna effect in the context of HBC.

In this paper, we present theoretical insights on the mechanism of HBC interference when the human body is exposed to RF electromagnetic plane waves in conjunction with investigation of the antenna effect of the human body on HBC operation. Expressions for the total induced axial current and the associated near-fields are derived for a cylindrical model of human body standing on a highly conductive infinite plane that is illuminated by a vertically polarised RF plane wave as shown in Fig. 1. Moreover, fields in the vicinity of the cylindrical model are calculated when there is HBC transmitter attached to the surface of the model. Finally, theoretical results are validated by empirical measurement and important results are discussed. Source points inside the cylinder model are identified with coordinates with prime symbol; and also, quantities inside and outside of the cylinder are identified with subscripts 1 and 2, respectively.

2. THEORY

2.1. Cylindrical Model of the Human Body

When the human body is illuminated by an electromagnetic plane wave, the total induced axial current in the body is less affected by the change in cross-sectional size and shape of the body provided that the tissue material is mainly conductive [12]. This explains the relatively higher specific absorption rate (SAR) in areas of the body where there is small conductive tissue mass or small cross-section area, such as the knee and ankle. Consequently, we used a homogenous cylindrical model of the body that comprises muscle tissue, which is the predominant tissue in the human body. The cylindrical human body model represents a standing posture with arms in contact with sides as shown in Fig. 1.

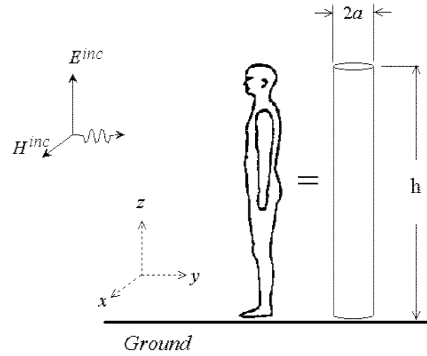


Figure 1. Cylindrical model of the human body exposed to vertically polarised plane wave.

The dielectric properties of biological tissues are frequency dependent that arise from dielectric dispersion due to the constituents of tissues at cellular and molecular levels [13]. The dielectric property of muscle can be approximated by Cole-Cole dispersions with parameters defined by Gabriel et al. [14]. The expression for the complex relative permittivity ϵ_{ω}^* as a function of excitation angular frequency ω is given as

$$\epsilon_{\omega}^* = \epsilon_{\infty} + \sum_{n=1}^4 \frac{\Delta\epsilon_n}{1 + (j\omega\tau_n)^{1-\alpha_n}} + \frac{\sigma_i}{j\omega\epsilon_0} \quad (1)$$

where n is the dispersion region identifier, ϵ_{∞} the permittivity at very large frequency, $\Delta\epsilon_n$ the strength of the dispersion, τ_n the relaxation time constant, α_n the distribution parameter that controls the width of the dispersion, σ_i the static ionic conductivity, and ϵ_0 the permittivity of free space. The complex conductivity σ_{ω}^* is calculated from (1) as

$$\sigma_{\omega}^* = j\omega\epsilon_0\epsilon_{\omega}^* = \sigma + j\omega\epsilon_0\epsilon \quad (2)$$

where σ is the conductivity and ϵ the relative permittivity.

Skin effect is taken into account by considering a time harmonic ($e^{j\omega t}$) and rotationally symmetric magnetic vector potential $A_{1z}(\rho, z)\hat{\mathbf{z}}$ maintained inside a very long and circular homogenous conducting cylinder of radius a that extends along the z -axis of a system of cylindrical coordinates (ρ, ϕ, z) . Solving the wave equation in the Lorenz gauge, the magnetic vector potential can be expressed as [15]

$$A_{1z}(\rho, z) = DJ_0(\kappa\rho) (C_1 \cos \gamma z + C_2 \sin \gamma z) \quad (3)$$

where D , C_1 , and C_2 are constants; J_0 is zeroth-order Bessel function, $\kappa^2 = k_1^2 - \gamma^2$, $k_1 = \sqrt{j\omega\mu_0\sigma_{\omega}^*}$ and $\gamma = \beta - j\alpha$ is the propagation constant along z -axis. The magnetic field inside the cylinder $B_{1\phi}$ is calculated as

$$B_{1\phi}(\rho, z) = -\frac{\partial A_{1z}(\rho, z)}{\partial \rho} = D\kappa J_1(\kappa\rho) (C_1 \cos \gamma z + C_2 \sin \gamma z). \quad (4)$$

If we assume the cylinder dimension satisfies the condition $k_2 a \ll 1$ ($k_2 = \omega\sqrt{\mu_0\epsilon_0}$ is the free space wave number) and it carries total axial current $I(z)$ that varies very slowly along the z -axis, then the

magnetic field on the surface can be approximated as [16]

$$B_{2\phi}(a, z) \simeq \frac{\mu_0 I(z)}{2\pi a}. \quad (5)$$

Enforcing the boundary condition of tangential magnetic field on the surface of the cylinder,

$$B_{1\phi}(\rho, z) \simeq \frac{\mu_0 I(z)}{2\pi a} \frac{J_1(\kappa\rho)}{J_1(\kappa a)} \quad (6)$$

provided that permeability of the cylinder is equal to that of the free space surrounding it, where J_1 is first-order Bessel function. Equation (6) implies that

$$I(z) = C_1 \cos \gamma z + C_2 \sin \gamma z. \quad (7)$$

For the case of the proposed human body cylindrical model that has finite length h , when it is totally illuminated by a vertically polarized plane wave, the total axial current should have a form similar to (7) with some modifications to compensate for the finite length.

The axial electric field inside the conductor can be calculated as

$$E_{1z}(\rho, z) = -j\omega \frac{\kappa^2}{k_1^2} A_{1z}(\rho, z) \simeq \frac{I(z)\kappa}{2\pi a\sigma_\omega^*} \frac{J_0(\kappa\rho)}{J_1(\kappa a)} \quad (8)$$

the impedance per unit length z^i of the cylinder is [15]

$$z^i = \frac{E_{1z}(a, z)}{I(z)} = \frac{\kappa}{2\pi a\sigma_\omega^*} \frac{J_0(\kappa a)}{J_1(\kappa a)} \quad (9)$$

and the volume current density $J_{1z}(\rho, z)$

$$J_{1z}(\rho, z) = \sigma_\omega^* E_{1z}(\rho, z) \simeq \frac{I(z)\kappa}{2\pi a} \frac{J_0(\kappa\rho)}{J_1(\kappa a)}. \quad (10)$$

The above expressions for field quantities of a very long cylinder are the basis for the analysis of the finite length cylindrical model of human body, which is treated in the next subsections.

2.2. Induced Axial Current in the Cylindrical Model

For our particular case, a time-harmonic ($e^{j\omega t}$) incident plane wave with electric field parallel to the axis of the z -directed cylinder of height h and radius a induces a current density distribution $\mathbf{J}_1(\mathbf{r})$ inside the cylinder. If the current density is known, the scattered magnetic vector potential outside the cylinder $\mathbf{A}_2(\mathbf{r})$ can be calculated in the Lorenz gauge as

$$\mathbf{A}_2(\mathbf{r}) = \frac{\mu_0}{4\pi} \int_{V'} \frac{\mathbf{J}_1(\mathbf{r}') e^{-jk_2 R}}{R} dv' \quad (11)$$

where $R = |\mathbf{r} - \mathbf{r}'|$ is the distance between observation and source points. We assume that the current density $\mathbf{J}_1(\mathbf{r})$ is rotationally symmetric in the cylindrical coordinate system (ρ, ϕ, z) , and, based on (10), it is approximated by the induced total axial current $I_{1z}(z)$ in the finite cylinder as

$$\mathbf{J}_1(\mathbf{r}) \simeq J_{1z}(\rho, z) \hat{\mathbf{z}} = \frac{I_{1z}(z)\kappa}{2\pi a} \frac{J_0(\kappa\rho)}{J_1(\kappa a)} \hat{\mathbf{z}}. \quad (12)$$

The dimension of the cylinder model loosely satisfies the *thin-wire antenna approximation* condition ($k_2 a \ll 1$ and $h \gg a$) for the frequency range of 1–200 MHz; thus, when the observation point is on the surface of the cylinder, the expression for R simplifies to

$$R \simeq \sqrt{(z - z')^2 + a^2}. \quad (13)$$

Therefore, the vector potential on the surface of the cylinder has only z -component,

$$A_{2z}(a, z) = \frac{\mu_0}{4\pi} \int_{-h}^h \int_0^a 2\pi J_{1z}(\rho', z') \rho' d\rho' dz' = \frac{\mu_0}{4\pi} \int_{-h}^h I_{1z}(z') \frac{e^{-jk_2 R}}{R} dz' \quad (14)$$

where the integration is carried out taking into account the cylinder image in the highly conductive ground. By enforcing boundary condition, the electric fields on the surface of the cylinder can be related as

$$\left(\frac{\partial^2}{\partial z^2} + k_2^2\right) A_{2z}(a, z) = \frac{jk_2^2}{\omega} (I_{1z}(z)z^i - V_0^e \delta(z) - E^{inc}) \quad (15)$$

where V_0^e is the potential difference on the load between the foot and the image in the ground with the electric field approximated by the *delta-gap* model, and E^{inc} is the incident electric field at the surface of the cylinder.

From (14) and (15), we derived approximate analytic expressions for the total axial current based on the King's three-term approximation for imperfectly conducting and loaded receiving cylindrical antenna as [17, 18]

$$I_{1z}(z) = V_0^e v(z) + U^{inc} u(z) \quad (16)$$

V_0^e and U^{inc} are defined as

$$V_0^e = -I_{sc}(0) \frac{Z_0 Z_L}{Z_0 + Z_L} \quad U^{inc} = \frac{E^{inc}}{k_2} \quad (17)$$

where $Z_0 = 1/v(0)$ is driving-point impedance of the same cylinder when base driven, Z_L is the load impedance, and $I_{sc}(0) = U^{inc} u(0)$ is current at the base when there is no load.

$$v(z) = \frac{j2\pi k_2}{\zeta_0 \gamma \Psi_{dR} \cos(\gamma h)} \left[\sin \gamma(h - |z|) + T_U (\cos \gamma z - \cos \gamma h) + T_D (\cos \frac{1}{2} k_2 z - \cos \frac{1}{2} k_2 h) \right] \quad (18)$$

$$u(z) = \frac{j4\pi}{\zeta_0} \left[H_U (\cos \gamma z - \cos \gamma h) + H_D (\cos \frac{1}{2} k_2 z - \cos \frac{1}{2} k_2 h) \right] \quad (19)$$

where $\zeta_0 = 120\pi \Omega$ is free space impedance. Both $v(z)$ and $u(z)$ have a form similar to the current in the long cylinder (7). The imperfectly conducting nature of the cylinder model is characterized by the parameter $\gamma = \beta - j\alpha$,

$$\gamma^2 = k_2^2 \left(1 - \frac{j4\pi z^i}{k_2 \zeta_0 \Psi_{dR}} \right). \quad (20)$$

The coefficients in (18) and (19) involve integrals that are computed numerically,

$$T_U = \frac{C_V E_D - C_D E_V}{C_U E_D - C_D E_U} \quad T_D = \frac{C_U E_V - C_V E_U}{C_U E_D - C_D E_U} \quad (21a)$$

$$H_U = \frac{C_D - E_D}{C_U E_D - C_D E_U} \quad H_D = \frac{E_U - C_U}{C_U E_D - C_D E_U} \quad (21b)$$

where

$$C_U = \left(1 - \frac{\gamma^2}{k_2^2} \right) (\Psi_{dUR} - \Psi_{dR}) (1 - \cos \gamma h) - \frac{\gamma^2}{k_2^2} \Psi_{dUR} \cos \gamma h + j \Psi_{dUI} \left(\frac{3}{4} - \cos \frac{1}{2} k_2 h \right) + \Psi_U(h) \quad (22a)$$

$$C_D = \Psi_{dD} \left(\frac{3}{4} - \cos \frac{1}{2} k_2 h \right) - \left(1 - \frac{\gamma^2}{k_2^2} \right) \Psi_{dR} (1 - \cos \frac{1}{2} k_2 h) + \Psi_D(h) \quad (22b)$$

$$C_V = - \left[j \Psi_{dI} \left(\frac{3}{4} - \cos \frac{1}{2} k_2 h \right) + \Psi_V(h) \right] \quad (22c)$$

$$E_U = - \frac{\gamma^2}{k_2^2} \Psi_{dUR} \cos \gamma h - j \frac{1}{4} \Psi_{dUI} \cos \frac{1}{2} k_2 h + \Psi_U(h) \quad (22d)$$

$$E_D = - \frac{1}{4} \Psi_{dD} \cos \frac{1}{2} k_2 h + \Psi_D(h) \quad E_V = j \frac{1}{4} \Psi_{dI} \cos \frac{1}{2} k_2 h - \Psi_V(h) \quad (22e)$$

$$\Psi_V(h) = \int_{-h}^h \sin \gamma(h - |z'|) \frac{e^{-jk_2 R_h}}{R_h} dz' \quad (23a)$$

$$\Psi_U(h) = \int_{-h}^h (\cos \gamma z' - \cos \gamma h) \frac{e^{-jk_2 R_h}}{R_h} dz' \quad (23b)$$

$$\Psi_D(h) = \int_{-h}^h \left(\cos \frac{1}{2} k_2 z' - \cos \frac{1}{2} k_2 h \right) \frac{e^{-jk_2 R_h}}{R_h} dz' \quad (23c)$$

$$\Psi_{dR} = \Psi_{dR}(z_m), \quad \begin{cases} z_m = 0, & k_2 h \leq \pi/2 \\ z_m = h - \lambda/4, & k_2 h > \pi/2 \end{cases} \quad (24a)$$

$$\Psi_{dR}(z) = \csc \gamma (h - |z|) \int_{-h}^h \sin \gamma (h - |z'|) \left[\frac{\cos k_2 R}{R} - \frac{\cos k_2 R_h}{R_h} \right] dz' \quad (24b)$$

$$\Psi_{dUR} = [1 - \cos \gamma h]^{-1} \int_{-h}^h [\cos \gamma z' - \cos \gamma h] \left[\frac{\cos k_2 R_0}{R_0} - \frac{\cos k_2 R_h}{R_h} \right] dz' \quad (24c)$$

$$\Psi_{dD} = \left[1 - \cos \frac{1}{2} k_2 h \right]^{-1} \int_{-h}^h \left[\cos \frac{1}{2} k_2 z' - \cos \frac{1}{2} k_2 h \right] \left[\frac{e^{-jk_2 R_0}}{R_0} - \frac{e^{-jk_2 R_h}}{R_h} \right] dz' \quad (24d)$$

$$\Psi_{dI} = - \left[1 - \cos \frac{1}{2} k_2 h \right]^{-1} \int_{-h}^h \sin \gamma (h - |z'|) \left[\frac{\sin k_2 R_0}{R_0} - \frac{\sin k_2 R_h}{R_h} \right] dz' \quad (24e)$$

$$\Psi_{dUI} = - \left[1 - \cos \frac{1}{2} k_2 h \right]^{-1} \int_{-h}^h [\cos \gamma z' - \cos \gamma h] \left[\frac{\sin k_2 R_0}{R_0} - \frac{\sin k_2 R_h}{R_h} \right] dz' \quad (24f)$$

$$R_0 = [z'^2 + a^2]^{\frac{1}{2}} \quad R_h = [(h - z')^2 + a^2]^{\frac{1}{2}} \quad (24g)$$

The value of γ is calculated by the process of iteration that is initialised by $\gamma = k_2$ to calculate z^i and Ψ_{dR} , which are in turn used to calculate γ . The iteration is found to be highly convergent; thus, the results after several iteration steps suffice to provide accurate approximation.

2.3. Fields due to Antenna Effect of the Cylindrical Model

The essence of HBC operation is signal transmission by maintaining electric potential distribution in the vicinity of the human body, where receiving units detect the signal from potential difference between two points located on the surface of the body or very close to the body. Therefore, it is relevant to introduce the fields produced in the vicinity of the human body due to electromagnetic field exposure, in this case a vertically polarized plane wave.

The magnitude of the volume charge density $\rho_{1v}(\rho, z)$ inside the cylinder can be related to the current density $J_{1z}(\rho, z)$ via a continuity equation as

$$\nabla \cdot J_{1z}(\rho, z) \hat{\mathbf{z}} = \nabla \cdot \frac{I_{1z}(z) \kappa J_0(\kappa \rho)}{2\pi a J_1(\kappa a)} \hat{\mathbf{z}} = -j\omega \rho_{1v}(\rho, z). \quad (25)$$

Enforcing the thin-wire approximation, fields very close to the cylinder can be approximately calculated by replacing the volume charge distribution with the total charge line density located on the axis of the cylinder [19]. Therefore, the radial electric field $E_{2z}(\rho, z)$ very close to the cylinder is approximated as

$$E_{2\rho}(\rho, z) \simeq \frac{1}{2\pi \epsilon_0 \rho} \int_0^a \rho_{1v}(\rho', z) \rho' d\rho' \int_0^{2\pi} d\phi' = \frac{j\zeta_0 I'_{1z}(z)}{2\pi k_2 \rho} \quad (26)$$

where $I'_{1z}(z)$ is first derivative of the current. Also, applying the thin-wire approximation, the magnetic field very close to the cylinder can be calculated replacing the volume current density distribution with the total axial current in a current filament located on the axis of the cylinder. Therefore,

$$B_{2\phi}(\rho, z) \simeq \frac{\mu_0 I_{1z}(z)}{2\pi\rho}. \quad (27)$$

The radial electric field inside the cylinder $E_{1\rho}(\rho, z)$ and the magnetic field inside the cylinder $B_{1\phi}(\rho, z)$ can be calculated from the vector magnetic potential maintained inside the cylinder $A_{1z}(\rho, z)$, which is approximated as

$$A_{1z}(\rho, z) \simeq -\frac{\mu_0 I_{1z}(z)}{2\pi a \kappa} \frac{J_0(\kappa\rho)}{J_1(\kappa a)}. \quad (28)$$

Therefore,

$$E_{1\rho}(\rho, z) = -\frac{j\omega}{k_1^2} \frac{\partial}{\partial\rho} \left(\frac{\partial A_{1z}(\rho, z)}{\partial z} \right) \simeq \frac{I'_{1z}(z)}{2\pi a \sigma_\omega^*} \frac{J_1(\kappa\rho)}{J_1(\kappa a)} \quad (29)$$

$$B_{1\phi}(\rho, z) = -\frac{\partial A_{1z}(\rho, z)}{\partial\rho} \simeq \frac{\mu_0 I_{1z}(z)}{2\pi a} \frac{J_1(\kappa\rho)}{J_1(\kappa a)}. \quad (30)$$

Using the thin-wire approximation, the external magnetic field in (27) represents the average total magnetic field close to the cylinder; therefore, the total axial electric field very close to the cylinder $E_{2z}(\rho, z)$ can be calculated from Faraday's law as

$$\frac{\partial E_{2z}(\rho, z)}{\partial\rho} = \frac{\partial E_{2\rho}(\rho, z)}{\partial z} + j\omega B_{2\phi}(\rho, z) \quad (31)$$

and the axial electric field inside the cylinder $E_{1z}(\rho, z)$ can be calculated as

$$E_{1z}(\rho, z) = \frac{J_{1z}(\rho, z)}{\sigma_\omega^*}. \quad (32)$$

Taking the value of axial electric field on the surface equal to $E_{1z}(a, z)$ from (32), the external total axial electric field simplifies to

$$E_{2z}(\rho, z) \simeq I_{1z}(z) z^i + \frac{j\zeta_0}{2\pi k_2} [I''_{1z}(z) + k_2^2 I_{1z}(z)] \ln\left(\frac{\rho}{a}\right) \quad (33)$$

where $I''_{1z}(z)$ is second derivative of the current. The scalar potential distribution very close to the surface of the cylinder can be calculated from the radial electric field as

$$\varphi_2(\rho, z) = \varphi_2(a, z) - \int_a^\rho E_{2\rho}(\rho, z) d\rho. \quad (34)$$

The scalar potential at the surface of the cylinder $\varphi_2(a, z)$ can be estimated from the internal axial vector potential $A_{1z}(\rho, z)$ using the Lorenz condition,

$$\varphi_2(a, z) = \varphi_1(a, z) \simeq -\frac{j\omega}{k_1^2} \frac{\partial A_{1z}(\rho, z)}{\partial z} \Big|_{\rho=a} = \frac{I'_{1z}(z)}{2\pi a \sigma_\omega^* \kappa} \frac{J_0(\kappa a)}{J_1(\kappa a)} \quad (35)$$

Therefore,

$$\varphi_2(\rho, z) \simeq \frac{I'_{1z}(z)}{2\pi} \left(\frac{1}{a\kappa\sigma_\omega^*} \frac{J_0(\kappa a)}{J_1(\kappa a)} - \frac{j\zeta_0}{k_2} \ln\frac{\rho}{a} \right). \quad (36)$$

2.4. Fields from HBC Transmitter Located on the Surface of the Cylindrical Model

The electromagnetic field produced by HBC transmitter situated on the surface of the body can be approximately analysed using the classic theory of electromagnetic fields from an elementary dipole source located above a plane conducting half-space. In particular, we considered a vertical electric dipole (VED) located at the surface of a homogenous, conducting, and semi-infinite media that has similar dielectric property to the cylinder model. It is well known that there are no suitable closed form solutions to the Sommerfeld integrals involved to evaluate fields near a dipole source. Thus, we adapted the approach of a finite conducting half-space image theory to calculate the quasi-static fields within the limit of distance much less than the free space wavelength [21, 22]. Basically, the idea of the finite conducting half-space image theory technique is to replace the imperfectly conducting half-space with a perfectly conducting half-space located at a complex depth $d/2$, where $d \simeq 2/k_1$. For the given frequency range of HBC operation, the domain of the quasi-static approach is appropriate for short distances in the vicinity of the body.

The charge oscillation between the body surface electrode and the circuit ground plane of the HBC transceiver can be represented by VED with the vertical orientation defined with respect to the axis of the cylinder model. We assumed that there is a fictitious current filament forming VED of moment Il at the center of the transmitter, where I is the current fed to the surface electrode and l is the small separation between the electrode and the ground plane.

Defining a new set of cylindrical coordinate with origin on the surface of the cylindrical model (assuming the cylindrical model is part of the half-space), the quasi-static fields at points not very close to the VED but at distances much less than the free space wavelength are approximated in [23] as

$$E_z(\rho, z) \simeq \frac{jIl\zeta_0}{2\pi} \left(\frac{1}{R_1^3} - \frac{3z^2}{R_1^5} \right) \quad (37a)$$

$$H_\phi(\rho, z) \simeq \frac{Il}{2\pi} \frac{\rho}{R_1^3} \quad (37b)$$

$$E_\rho(\rho, z) \simeq \frac{jIl\zeta_0\rho}{4\pi} \left[\frac{6z}{R_1^5} \left(1 - \frac{k_2^2}{k_1^2} \right) - \frac{k_2^2}{\rho^2} \left(\frac{z+d}{R_2} - \frac{z}{R_1} \right) \right] \quad (37c)$$

where R_1 is distance between the dipole and observation point, and R_2 is distance from the image dipole to the observation point

$$R_1 = \sqrt{\rho^2 + z^2} \quad R_2 = \sqrt{\rho^2 + (z+d)^2}. \quad (38)$$

It is well known that the magnetic vector potential in the air region for VED located on the surface of lossy half-space is given as

$$\mathbf{A}(\mathbf{r}) = A_z(\rho, z)\hat{\mathbf{z}} = \frac{\mu_0 Il}{4\pi} \left(\frac{e^{-jk_2 R_1}}{R_1} - \int_0^\infty \frac{e^{-u_2 z}}{u_2} \frac{\tau^2 u_1 - u_2}{\tau^2 u_1 + u_2} J_0(\lambda\rho) \lambda d\lambda \right) \hat{\mathbf{z}} \quad (39)$$

where

$$u_2 = \sqrt{\lambda^2 - k_2^2} \quad u_1 = \sqrt{\lambda^2 - k_1^2} \quad \tau = \frac{k_2}{k_1} \quad (40)$$

The integral in (39) characterizes the effect of the lossy ground; therefore, based on the finitely conducting half-space image theory, it can be approximated by the contribution of the image dipole located at the complex depth of d . So that, the quasi-static scalar electric potential can be approximated in the Lorenz gauge as

$$\varphi(\rho, z) = \frac{j\omega}{k_2^2} \frac{\partial A_z(\rho, z)}{\partial z} \simeq -\frac{jIl\zeta_0}{4\pi k_2} \left(\frac{z}{R_1^3} + \frac{z+d}{R_2^3} \right). \quad (41)$$

2.5. Conducted Interference in HBC Receivers

In addition to the HBC scenario mentioned previously, there is another promising application area of HBC where the receiving circuit is embedded externally in the surrounding environment of human body; and a closed circuit path is established when the subject wearing a transmitter touches or gets very close to the receiver electrode. The receiver detects the signal from the potential difference between the contact electrode and the ground. For this case, in addition to the interference caused by fields in the vicinity of the body, there is also conducted interference due to the induced current in the body — part of the current induced in the body from electromagnetic fields exposure gets grounded via the receiver circuit.

We analysed this problem by segmenting the cylinder into two parts, cutting it at $z = z_t$ as shown in Fig. 2. We treated the two segments as separate parasitic cylindrical antennas. The upper segment generates current at $z = z_t$ with source voltage of V_{oc}^u and output impedance of Z_0^u ; and the lower segment and the receiver act like a load. The lower segment also generates current at the foot of the cylinder ($z = 0$) with source voltage V_{oc}^l and output impedance of Z_0^l as shown in Fig. 2(b).

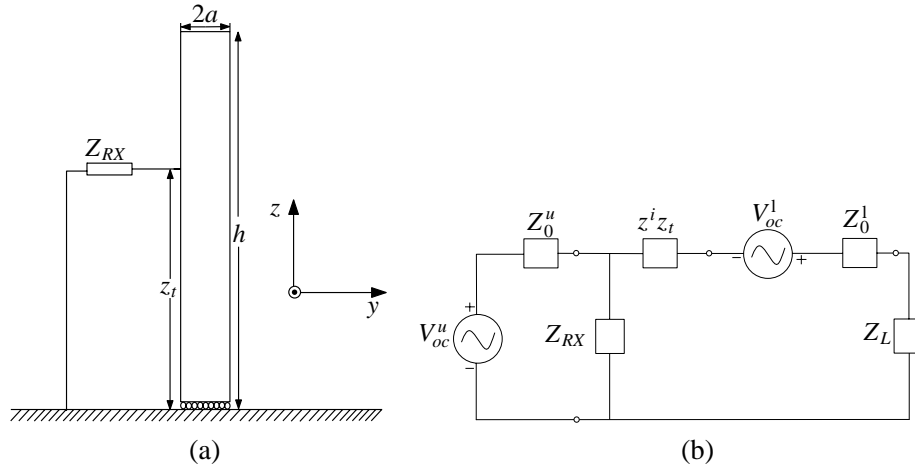


Figure 2. Human body cylinder model with externally embedded HBC receiver. (a) Cylinder with parallel load. (b) The corresponding equivalent circuit.

The upper segment source voltage V_{oc}^u is calculated by shorting the load as

$$V_{oc}^u = I_{sc}^u Z_0^u \tag{42}$$

where I_{sc}^u and Z_0^u are calculated based on the approach described in Section 2.2, but taking the new height of the cylinder as $h_u = h - z_t$. The same applies for calculation of the lower source voltage V_{oc}^l and the corresponding impedance Z_0^l . Therefore, the current in the receiver load impedance I_{RX} can be calculated as

$$I_{RX} = \frac{Z_{eq}}{Z_{RX}} \left[\frac{V_{oc}^l Z_0^u + Z_{RX} (V_{oc}^l + V_{oc}^u)}{Z_0^u Z_{eq} + Z_{RX} (Z_{eq} + Z_0^u)} \right] - \frac{V_{oc}^l}{Z_{RX}} \tag{43}$$

where $Z_{eq} = z^i z_t + Z_0^l + Z_L$, and Z_L is impedance between the sole of the foot and the image.

3. RESULTS AND DISCUSSION

The objective of this paper was to introduce the theoretical mechanism of interference in HBC as well as human body antenna effects on HBC operation, as there is a gap in the explanation of phenomena occurring in HBC. The complete characterization of HBC requires solving Maxwell’s equation inside a high resolution voxel model of the human body as well as simulation of realistic near-field sources of interference that are more likely to be encountered in real-life. Such an approach calls for high computation time and complexity; therefore, we presented a simpler but useful approach to characterize

HBC interference. The analytic solution derived for the total axial current, which is based on King's three-term approximation, is reasonably accurate for the cylindrical model of the body. The actual human body has varying cross-sectional area due to different tissue layers, body parts and body postures; thus, the cylindrical model roughly approximates the case of a standing position with arms in contact with sides. Since the fields in the vicinity of the model are functions of the total axial current, we confine our discussion to the total axial current that can be easily related to the near-fields based on the relations outlined in the previous sections. The total axial current derived is a function of the dielectric property of the material forming the cylindrical model, the incident field, dimension of the model and the load at the foot. This is based on the implicit assumption that the ground is perfectly conductive and there are no nearby objects that rescatter the near-field.

The calculation of fields near the cylinder model in Section 2.3 is valid for distances very close to the cylinder $\rho < 10a$ [19]. The total axial current for unloaded case ($Z_L = 0$), as well as the magnetic field close to the cylinder, which does not involve a derivative of the total axial current, are excellent approximations. Nevertheless, the use of nonzero load and derivatives of the total axial current in the calculation of fields compromise the accuracy near the foot and edge of the cylinder, respectively. The accuracy of the axial electric field close to the cylinder can be improved by using a first-order iteration of the total axial current as pointed out in [20].

3.1. The Effect of h and Z_L on the Induced Total Axial Current

It is well known that a thin and perfectly conducting wire antenna has a narrowband frequency response. On the other hand, a thick and imperfectly conducting antenna, such as the cylinder model we used, has a broadband frequency response within the HBC frequency range [24]. This implies that different radiation sources operating within the HBC frequency range, including nearby HBC users, have the potential to cause interference to HBC devices on which low power operation is intrinsic. For example, in typical healthcare settings, different devices use high frequency narrowband energy for their operation that falls within HBC frequency range; MRI uses 64 MHz sources, and lasers often use 13- or 27-MHz sources. Also other major sources of EMI include intentional radiators such as, telemetry and paging transmitters, and handheld radios.

The frequency response of the cylinder model also has a first resonance within the HBC frequency range, which shifts depending on the height of the cylinder h and the load at the foot Z_L . As the height increases from 1.5 m to 2 m, the resonance frequency shifts from 45 MHz to 35 MHz, as shown in Fig. 3(a), given that the impedance between the foot and the image is zero. The calculated resonance frequencies are in good agreement with the resonance frequencies of whole-body-averaged SAR predicted by other authors, such as Dimbylow [25], using FDTD algorithm on voxel-based models of real human anatomy. A good summary of related works by other authors is compiled in [26]. The presence of a load on the base of the cylinder has effect on the resonance frequency as well as the magnitude of the induced axial current. Assuming the load at the base of the cylinder is due to the impedance of rubber ($\epsilon = 3.5$) sole shoes, increasing the thickness of the sole introduces other resonances at higher frequencies while

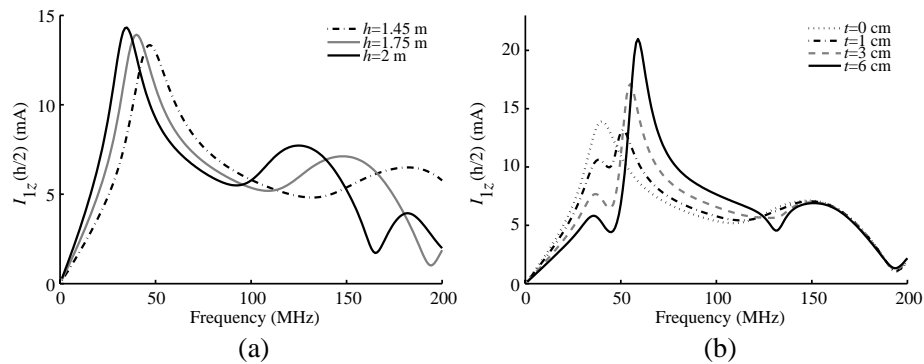


Figure 3. The effect of height h and load Z_L on the total axial current for $E^{inc} = 1$ V/m. (a) $I_{1z}(h/2)$ for different height of cylinder. (b) $I_{1z}(h/2)$ for different thickness of the rubber sole.

decreasing the magnitude of the first resonance occurred due to change in the height of the cylinder, Fig. 3(b).

3.2. Variations of the Potential Difference at the Electrodes of on-Body HBC Receiver

As pointed out earlier, the HBC receiver detects the signal from the electric potential difference established between two points. In order to see how the received signal is affected by interference, we considered a transmitter and receiver that has 2 cm radius and 2 cm separation between their surface electrodes and circuit ground planes. We assumed that the transmitter feeds the electrode 1 mA current and is located on the surface of the cylinder at $(a, 0, h/2)$ in the coordinate system of the cylinder model. Implementing quasistatic approximation, the signal detected by the receiver, which is located at $(a, 0, z)$, is calculated from the scalar potential difference between points on the surface of the cylinder and points 2 cm farther on the same radial line $(a + 0.02, 0, z)$. In reality, since the receiver is located in the reactive near-field of the transmitter and acts as a load to the transmitter, the current fed to the transmitter varies according to the location of the receiver. For the sake of simplicity, we assumed that the current remains constant and independent of the location of the receiver. The scalar potential in (36) is a function of first derivative of the current, which implies that the electric potential difference on the receiver, in the presence of a plane wave, is affected by location of the receiver, the load at the foot Z_L , and magnitude and frequency of the field E^{inc} . As discussed previously, Z_L introduces resonance such that the potential difference is much more affected near the resonance frequency. Fig. 4(a) shows the effect of Z_L on the potential difference distribution along the length of the cylinder. The relationship between magnitude of E^{inc} and the calculated potential difference is obvious; the potential difference due to the plane wave is directly proportional to E^{inc} and its influence on the potential difference is shown in Fig. 4(b).

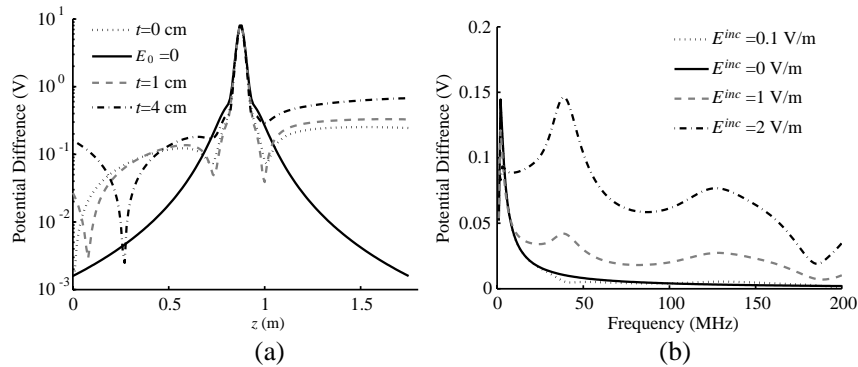


Figure 4. The effect of load and magnitude of the plane wave on the potential difference. (a) Electric potential difference on the surface of the cylinder for different thickness of the rubber sole. (b) Effect of $|E^{inc}|$ on the potential difference at $z = h/2 - 0.3$ from the transmitter located at $z = h/2$.

3.3. The Effect of the Human Body as Transmitting Antenna

The analysis in Section 2.4 is based on the assumption that the human body is represented by infinite conductive half-space; but it does not take into account the characteristics of the human body as a transmitting cylindrical antenna. Assuming that HBC transmitter acts like a source that drives current into the human body, the expression in (16) can be used to characterize the total induced axial current in the cylinder model for the particular case of the transmitter located at the base of the cylinder. The voltage at the base V_0^e , in this case, includes an additional term that represents the driving voltage of the HBC transmitter. This hypothesis is verified by a simple measurement using a battery powered vector network analyser (VNA) as shown in Fig. 5(a). In the literature, different theoretical HBC system models are validated using measurements on the arm. In order to complement the existing results in the literature, we carried out measurements on a human subject (1.73 m height) whose arm has length

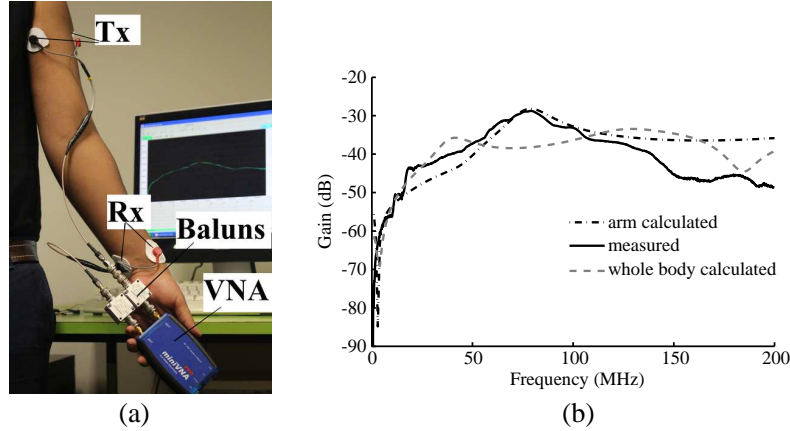


Figure 5. Gain measurement setup and gain measured and calculated results. (a) Gain measurement setup. (b) Measured and calculated gain results.

of 70 cm and average radius of 5 cm. The VNA is set to sweep a constant interval frequency of range 1–200 MHz with 0 dBm output power, which is well below the safety limit set by International Commission on Non-Ionizing Radiation Protection (ICNIRP) [27]. The signal is coupled to the upper arm using a pair of Ag/AgCl electrodes; and the VNA detects the potential difference across a pair of Ag/AgCl electrodes located 40 cm farther on the lower arm. Baluns are used to isolate the common ground circuit plane of the transmitting and receiving ports of the VNA so that the return path through the VNA is avoided. The measured gain is maximum near 80 MHz as shown in Fig. 5(b). A good approximation to the measurement result can be obtained by representing the arm by a cylindrical antenna of $h = 70$ cm and $a = 5$ cm, which is driven at its base and has resonance near 80 MHz, by assuming that the rest of the body acts like ground plane. The gain is calculated using the potential difference at $z = 2$ cm as the input voltage and the potential difference at $z = 40$ cm as the output voltage. The calculation result points to the possibility that the maximum gain near 80 MHz could be due to the resonance of the arm. Moreover, the measurement results show that the resonance frequency is not affected by the position of the electrodes; rather, only the gain is directly linked to the separation between the transmitting and the receiving electrodes. If the receiving electrodes are located at 30 cm farther from the transmitting electrodes, the gain increases by approximately 2 dB. In relation to this, some authors reported gain measurements that has maximum near 50 MHz. If we assume that the cylinder model has a dimension comparable to that of whole human body, the resonance occurs near 50 MHz for the case of $h = 1.75$ m as shown in Fig. 5(b), depending on the load at the foot. This suggests that the gain peak near 50 MHz could be due to the resonance of the whole body. Moreover, assuming that the ground is well insulated so that the image cylinder in the ground is not considered, the length of the antenna is halved resulting in a shift of the resonance frequency between 60–75 MHz, depending on the height of the cylindrical model.

3.4. The Current Conducted to Externally Embedded HBC Receiver

For the purpose of inspecting the validity of the approach we proposed in Section 2.5, a human subject of 1.73 m height is illuminated by an electromagnetic field from a 60 cm monopole antenna located 3 m away as shown in Fig. 6(a). The monopole antenna is fed by a battery powered RF source tuned to generate 1–200 MHz at 0 dBm. An AC-powered benchtop spectrum analyser measures the power in the electric current established when the subject touches a metallic electrode of 1.5 cm radius that is connected to the spectrum analyser port via a 3 cm coaxial cable. Even though it is known that, at the given distance, the incident electric field is not a perfect plane wave due to superposition of other components e.g. reflections, the proposed theoretical approach predicted the measured power to a reasonable accuracy as shown in Fig. 6(b). The value of the incident electric field is calculated based on the formula for vertical electric near-field of a monopole antenna of height h and base current $I(0)$

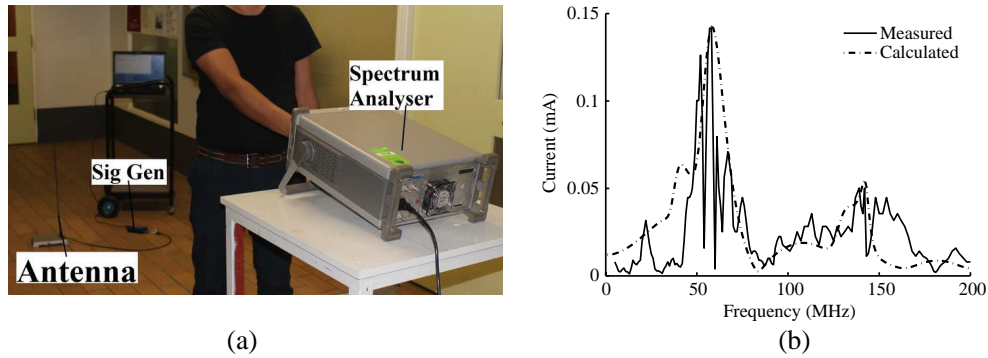


Figure 6. Measurement setup and measured and calculated current in mA when a subject touches an electrode attached on spectrum analyser. (a) Current measurement setup. (b) Measured and calculated current in mA.

as

$$E^{inc} \simeq \frac{jI(0)h}{4\pi\omega\epsilon_0\rho^3}(1 + jk_2\rho) \quad (44)$$

where $h = 0.6$ m and $\rho = 3$ m. The calculation result indicates that the resonance between 50–70 MHz occurred due to the load at the foot Z_L ; the small resonance near 75 MHz could possibly be due to the resonance of the arm; and the receiver load Z_{RX} , which is the hand-electrode contact impedance and impedance of the network analyser that acts as high pass filter suppressing the low frequency components.

3.5. General Remarks

The choice of operation frequency in HBC is a trade-off between gain and interference. For example, near 50 MHz better gain performance can be obtained that leads to better communication performance but at the same time it might also increase the risk of interference to other HBC users or from nearby devices operating at the same frequency. For applications that the user is isolated from other users and electronic devices, the frequency near 50 MHz or 80 MHz gives a better gain performance. For applications where require communication between nearby HBC users, center frequencies near 50 MHz might be promising with respect to low power requirement.

The interference due to RF exposure of the human body gets exacerbated by the dynamic nature of the human body. The human body is not stationary; it can get close to other EMI sources, which increases the level of induced current in the body. This implies that the design of HBC transceiver should take into account the mobility of human body as well as the likely EMI sources that can be encountered and their maximum field so that robust source, channel codings and modulation techniques can be deployed. Moreover, the HBC design should also consider EMI due to HBC devices on other body worn or implanted devices. In relation to this, HBC devices should also comply with Electromagnetic Compatibility (EMC) legislations. For example, the European Union EMC directive requires that a device should be immune to certain level of interference to work as intended. To get a quality label on an electronic device the directive imposes that the device should not malfunction when exposed to an electric field of 3 V/m up to 1 GHz.

4. CONCLUSION

The effect of the human body as an antenna on HBC is investigated. A homogenous cylindrical model of the human body is proposed, with electrical properties similar to muscle tissue. The induced total axial current in the model when it is exposed to plane waves is derived, which can be easily modified when the HBC transmitter is assumed to drive the human body as an antenna. Expressions for electromagnetic fields very close to the cylinder are derived when the cylindrical model is illuminated by plane wave as well as when HBC transmitter is located on the surface of the cylinder. The effect of conducted

interference, when the HBC receiver is located externally, is investigated using the cylindrical antenna model of the body. The calculation of potential difference revealed the cause of important phenomena in HBC gain measurements — the peaks occurring near 80 MHz and 50 MHz, which could be due to resonance of the arm or whole body, respectively. The selection of frequency in HBC transceiver design should not only rely on the gain performance, but it should also take into account the interference caused by the human body antenna effect.

REFERENCES

1. Wang, J. and Q. Wang, *Body Area Communications: Channel Modeling, Communication Systems, and EMC*, John Wiley & Sons, Somerset, NJ, USA, 2013.
2. Seyedi, M., B. Kibret, T. H. D. Lai, and M. Faulkner, "A survey on intrabody communications for body area network applications," *IEEE Trans. Biomed. Eng.*, Vol. 60, No. 8, 2067–2079, 2013.
3. Xu, R., H. Zhu, and J. Yuan, "Electric-field intrabody communication channel modeling with finite-element method," *IEEE Trans. Biomed. Eng.*, Vol. 58, No. 3, 705–712, 2011.
4. Cho, N., J. Yoo, S. Song, J. Lee, S. Jeon, and H. Yoo, "The human body characteristics as a signal transmission medium for intrabody communication," *IEEE Trans. Microw. Theory Tech.*, Vol. 55, No. 5, 1080–1086, 2007.
5. Cho, N., J. Lee, L. Yan, J. Bea, S. Kim, and H. Yoo, "A 60 kb/s-to-10 Mb/s 0.37 nJ/b adaptive-frequency-hopping transceiver for body-area network," *IEEE J. Solid-State Circuits*, Vol. 44, No. 3, 708–717, 2009.
6. Wang, Q., T. Sanpei, Q. Wang, and D. Plettemeir, "EMI modeling for cardiac pacemaker in human body communication," *Proc. Int. Symp. on EMC*, 629–632, 2009.
7. Park, H., I. Lim., S. Kang, and W. Kim, "Human body communication system with FSBT," *Proc. IEEE ISCE*, 1–5, 2010.
8. Anguera, P. J., D. Aguilar, J. Vergés, M. Ribó, and C. Puente Baliarda, "Handset antenna design for FM reception," *Proceedings of the IEEE Antennas and Propagation Society International Symposium*, 1–4, 2008.
9. Aguilar, D., P. J. Anguera, C. Puente Baliarda, and M. Ribó, "Small handset antenna for FM reception," *Microwave and Optical Technology Letters*, Vol. 50, No. 10, 2677–2683, 2008.
10. Vergés, J., P. J. Anguera, C. Puente Baliarda, and D. Aguilar, "Analysis of the human body on the radiation of FM handset antenna," *Microwave and Optical Technology Letters*, Vol. 51, No. 11, 2588–2590, 2009.
11. Pladevall, A., C. Picher, A. Andújar, and P. J. Anguera, "Some thoughts on human body effects on handset antenna at the FM band," *Progress In Electromagnetics Research*, Vol. 19, 121–132, 2011.
12. Poljak, D., *Human Exposure to Electromagnetic Fields*, WIT Press, Ashurst, Southampton, UK, 2004.
13. Foster, K. R. and H. P. Schwan, "Dielectric properties of tissues and biological materials: A critical review," *Crit. Rev. Biomed. Eng.*, Vol. 17, No. 1, 25–104, 1989.
14. Gabriel, S., R. Lau, and C. Gabriel, "The dielectric properties of biological tissues: III. Parametric models for the dielectric spectrum of tissues," *Phys. Med. Biol.*, Vol. 41, No. 11, 2271–2293, 1996.
15. King, R. W. P. and S. Prasad, *Fundamental Electromagnetic Theory and Applications*, Prentice-Hall, Englewood Cliffs, USA, 1986.
16. King, R. W. P. and T. T. Wu, "Currents, charges, and near fields of cylindrical antennas," *Radio Science Journal of Research NBS/UNSC-URSI*, Vol. 69D, No. 3, 429–446, 1965.
17. King, R. W. P. and T. T. Wu, "The imperfectly conducting cylindrical transmitting antenna," *IEEE Trans. Antennas Propag.*, Vol. 14, No. 5, 524–534, 1966.
18. Taylor, C. D., W. H. Charles, and A. A. Eugene, "Resistive receiving and scattering antenna," *IEEE Trans. Antennas Propag.*, Vol. 15, No. 3, 371–376, 1967.

19. King, R. W. P. and T. T. Wu, "Electromagnetic field near a parasitic cylindrical antenna," *Proc. Inst. Electr. Eng.*, Vol. 113, No. 1, 35–40, 1966.
20. King, R. W. P. and T. T. Wu, "Currents, charges, and near fields of cylindrical receiving and scattering antennas," *IEEE Trans. Antennas Propag.*, Vol. 13, No. 6, 978–979, 1965.
21. Wait, J. R. and K. P. Spies, "On the image representation of the quasi-static fields of a line current source above the ground," *Can. J. Phy.*, Vol. 47, No. 23, 2731–2733, 1969.
22. Wait, J. R., "Image theory of a quasistatic magnetic dipole over a dissipative half-space," *Electron. Lett.*, Vol. 5, No. 13, 281–282, 1969.
23. Bannister, P. R., "Summary of image theory expressions for the quasi-static fields of antennas at or above the earth's surface," *Proc. IEEE*, Vol. 67, No. 7, 1001–1008, 1979.
24. Balanis, C. A., *Antenna Theory: Analysis and Design*, John Wiley & Sons, New Jersey, USA, 2005.
25. Dimbylow, P. J., "Fine resolution calculations of SAR in the human body for frequencies up to 3 GHz," *Phys. Med. Biol.*, Vol. 47, No. 16, 2835–2846, 2002.
26. Hand, J. W., "Modelling the interaction of electromagnetic fields (10 MHz–10 GHz) with the human body: methods and applications," *Phys. Med. Biol.*, Vol. 53, No. 16, R243–R286, 2008.
27. ICNIRP (International Commission on Non-Ionising Radiation Protection), "Guidelines for limiting exposure to time-varying electric, magnetic, and electromagnetic fields (up to 300 GHz)," *Health Phys.*, Vol. 74, No. 4, 494–522, 1998.